ORIGINAL PAPER

The Effect of Tunnel Geometry and Geomechanical Parameters of Host Rock on Tunnel Displacement Profile

Mohammad Ghaffari · Saeed Mahdevari

Abstract Examination of tunnel displacement profile is one of the basic requirements in tunnel design which controls the internal forces of the lining and the surface settlements. The previous studies on the tunnel displacement profile have been in the form of elastic analysis and do not consider changes in the overburden and geomechanical parameters of the host rock. Therefore, using three-dimensional numerical simulation, this study has investigated the effect of tunnel diameter, overburden and geomechanical parameters of the host rock on the tunnel displacement profile. The results of analysis showed that the average displacement occurred in the face for diameters of 7 and 10 m was 27 and 26% of total displacement, respectively, and its value was directly related to cohesion and inversely related to overburden. The tunnel overburden as well as its diameter are the main factors in determining the location where 5 and 95% of total displacement take place while cohesion influences only the 5% location of total displacement while the deformation modulus had no effect on the displacement profile. The displacement profile proposed by Hoek was fitted to the profile extracted from numerical simulation. The relationship between the overburden, diameter, and geomechanical parameters of the host rock and the fixed coefficients of the proposed Hoek function was also evaluated, and equations were proposed to estimate the fixed coefficients of the function.

Keywords Tunnel displacement profile · Three-dimensional numerical simulation · Tunnel face displacement · Tunnel design

1 Introduction

The population growth makes the development of public transport in metropolitan areas inevitable. Facing urban facilities and the impossibility of land acquisition in dense urban environments have turned the construction of underground urban train tunnels into an accepted solution from technical, economic, and safety points of view in metropolitan areas. The tunnel displacement profile and the distance from the tunnel where the maximum subsidence occurs are notable points in tunnel construction. The deformation of a tunnel starts from about twice the tunnel diameter behind the face and increases with the progress of the face, finally converging to a maximum value, which is not influenced any by the face anymore (Hoek 1999). A key point in the tunnel displacement profile is the amount of displacement in the tunnel face, which has

M. Ghaffari · S. Mahdevari (✉)
Department of Mining Engineering, Isfahan University of Technology, Isfahan, Iran
e-mail: smahdevari@iut.ac.ir

M. Ghaffari
e-mail: mghaffari@mi.iut.ac.ir

been reported to be 25–30% of the total tunnel displacement (Carranza-Torres and Fairhurst 2000; Unlu and Gercek 2003). The amount of displacement on the tunnel face is important since it controls the minimum expected settlement at the ground surface and when face displacement increases, the surface subsidence will increase (Ocak 2008). The amount of displacement in the face also controls the amount of ground loss in mechanized excavation (Attewell et al. 1986). The tunnel displacement profile also controls the amount of load applied to the installed temporary or permanent support. The minimum support installation distance from the face is controlled by the tunnel excavation cycle in drill and blasting technique or machine specification in mechanized excavation. A basic parameter that is effective in choosing full-face single-shield and double-shield excavation machines is the required thrust, which is measured according to the machine diameter, tunnel diameter, tunnel displacement profile, and ground response curve. A study by Unlu and Gercek on the effect of the Poisson's ratio on the displacement around a tunnel showed that experimental equations could be obtained to predict normalized radial deformations used in the in-situ hydrostatic stress field (Unlu and Gercek 2003). Torres and Fairhurst studied the deformation profile of a tunnel affected by tunneling and evaluated the tunnel displacement with respect to the face displacement and the tunnel diameter (Carranza-Torres and Fairhurst 1999). Numerous numerical analyses have been performed to determine the rock response to twin tunnels excavated at shallow (Rahim et al. 2015; Chakeri et al. 2011; Do et al. 2014; Hasanpour et al. 2012) and deep (Addenbrooke and Potts 2001; Chen et al. 2009; Ghaboussi and Ranken 1977) depths. Wang et al. proposed a group of analytical solutions to evaluate the displacements and stresses produced when two nearly situated circular tunnels are consecutively built in viscoelastic rock (Wang et al. 2017). Wang et al. also introduced a novel analytical solution by which the ground responses near shallow circular tunnels subjected to surcharge loads could be rapidly anticipated. The ground was approximately assumed a viscoelastic or elastic medium, and the random distribution of surcharge loads was regarded as a viscoelastic model (Wang et al. 2018). Zheng et al. (2019) developed an easy method to estimate the uplift of underground structures. Moussaei et al. designed and constructed a model setup to simulate the

excavation process of a circular full-face tunnel using the change in tunnel caused by the lost volume. Particle Image Velocimetry was used to control the ground deformation during the excavation procedure. A new experiential relation was presented to forecast the highest settlement of ground as a function of ground density (Moussaei et al. 2019). Wang et al. used multi-point extensometers which were placed in Beishan Exploration Tunnel in Gansu Province of China before excavation to perform an in-situ controlling experiment on the surrounding rock's internal displacement (Wang et al. 2019). Lu et al. suggested a displacement function of the shallow circular tunnel cross-section stated by the Fourier series. Case studies of Docklands Light Railway Lewisham Extension were used to prove the applicability and capacity of the suggested solution, which was found to be an easy way to assess the tunnel deformation during compound construction and geological conditions (Lu et al. 2019). Zeng et al. represented novel analytical solutions for a step-by-step excavation of tunnel cross-sections, arbitrary tunnel shapes, the ground's viscoelastic properties, and pressures applied at the internal boundaries of tunnel caused by water or liner pressures (Zeng et al. 2020). Centrifuge modeling has been employed as a means to investigate soil movements affected by tunneling and its interactions with existing structures. In 2D plane-strain centrifuge models, loss of tunnel volume can be simulated in various ways. Song and Marshall sought to address this issue using conflicting results of plane-strain centrifuge experiments employing a flexible membrane tunnel model and those of a recently developed unconventional mechanical model of tunnel rigid boundary. The results help to understand which tunnel model type can be used in centrifuge tests for the 2D plane-strain modeling of tunnels (Song and Marshall 2020). Zheng et al. defined the vital effects of yaw excavation loadings on segmental stress and ground displacement for a curved shield tunnel. The tangential compressive stress, axial tensile stress, and axial compressive stress of recently mounted curve-line tunnel segments were more than those of the straight tunnel. The stress levels linearly rose with yaw (Zhang et al. 2020). Yertutanol et al. performed vertical displacement controlling and verification together with primary support design for Konak twin-tube tunnel in İzmir. It was perceived that neither the rock nor the mass of support system elements had yielded

because of the redistribution of stresses caused by the disturbance due to the tunnel excavation (Yertutanol et al. 2020). Lu et al. (2020) presented a unified time-dependent displacement function using a Fourier series as the tunnel cross-section's displacement control boundary condition. Gao et al. (2021) expressed a new analytical solution for the displacement and stress near circular lined tunnels at a shallow depth regarding the interaction between the rigid lining, ground, and distributed surcharge loading. Kong et al. expressed a stress function using the Fourier series to consider the complex stress state of the medium of a shallow tunnel under water. A fractional viscoelastic solution was defined according to the attained elastic solution using the correspondence standard. The time-dependent displacement of ground was studied regarding the stress release influence (Kong et al. 2021). Zheng et al. suggested a new probabilistic process to estimate the uncertainty of tunnel displacement and properties of the rock mass that incorporated a relevance vector machine and multivariate distribution function. It was observed that the anticipated displacements of the tunnel by the relevance vector machine model were highly compatible with the observed ones. The factors' correlation had substantial influences on the uncertainty results. The uncertainty of tunnel displacement declined, whereas the tunnel reliability grew with the rises in the negative correlations between rock mass factors. Compared to the deterministic technique, the suggested method was more scientific and rational while being compatible with rock engineering applications (Zheng et al. 2021).

A review of the studies on the tunnel displacement profiles reveals that the effect of geometry and geomechanical parameters of the host rock on the tunnel displacement profile has not been comprehensively investigated so far. Tunnel displacement profile is one of the basic requirements in tunnel design, and the existing displacement profiles are also based on elastic analysis. So in this research, applying 3D numerical simulation and Mohr–Coulomb elastoplastic model as a popular constitutive model in geomechanics, the effect of overburden, tunnel diameter, and geomechanical parameters of the host rock on the tunnel displacement profile was evaluated. Then the tunnel displacement profiles extracted from numerical simulation have been compared with tunnel displacement profile purposed by Hoek and three equations

have been developed to estimate the coefficients of Hoek's displacement profile based on geotechnical parameters of the host rock and tunnel geometry.

2 Methodology

2.1 Numerical Simulations

In the numerical simulation, the Mohr–Coulomb elastoplastic criterion was employed, which is a well-known criterion used in geomechanics. The diameter of the tunnel was 7 and 10 m, and three overburdens of 50, 250, and 500 m were selected for numerical simulation. Choosing overburden within this range allows for studying the displacement profile in shallow and deep tunnels. Table 1 lists the ranges of the geomechanical parameters used in the numerical simulation.

In order to eliminate the boundary effects on the numerical simulation results, the dimensions of the model in the X, Y, and Z directions were selected as 100 m, and the tunnel was excavated in the Y direction. The bottom boundary of the model was fixed in all three directions, and roller supports were used in the lateral boundaries located in the X and Y directions. In 250 and 500 m overburden, the remaining weight of the overburden was calculated and applied in the form of stress in the Z direction at the upper boundary of the model. The principal stresses were considered in horizontal and vertical directions (Fig. 1).

2.2 Discussion

2.2.1 The Effect of Changes in Geomechanical Parameters, Diameter, and Overburden on the Occurrence Location of 95 and 5% of the Total Displacement

Due to the changes in the overburden and geomechanical parameters, the tunnel displacement had different values, and it is not possible to compare them in this way. Therefore, the displacements in the tunnel crown were normalized relative to their maximum values, and the tunnel displacement profiles were plotted against the distance from the face. In this way, the displacement was comparable in all models, varying from 0 to 100%, and the displacement profile

Table 1 The ranges of changes in geomechanical parameters used in the numerical simulation

Poisson's ratio	Friction angle (°)	Young modulus (GPa)	Cohesion (kPa)
0.3	25–35	1.5–5	300–1000
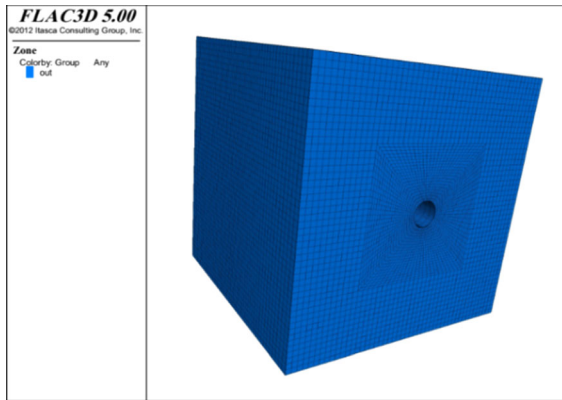
Fig. 1 The geometry of the numerical model

could be compared and reviewed. Analytical equations that fit the displacement profile do not suggest a finite range for displacement from 0 to 100%, and the range is infinite. Therefore, in order to provide the possibility of comparing the results of the numerical method with those of the analytical methods and make analysis easier, the displacement range of 5–95% was considered the basis of the analysis.

It is necessary to know the occurrence range of 5–95% of the displacement due to its effect on the surface subsidence and the way the extension and compression zones are converted to each other, especially in twin tunnels. In order to investigate the effect of variable parameters used in numerical simulation on the occurrence range of 5–95% of tunnel displacement, analysis of variance was used. The results obtained for the location of 95% displacement are shown in Table 2. For a significant relation with a confidence level of 95%, the P-value has to be less than 0.05. Hence, according to the results, there was no significant relationship between the deformation modulus and the location of 95 and 5% displacement.

The occurrence location of 5 and 95% of the displacement relative to the tunnel face, which was normalized relative to the tunnel diameter, is shown against the overburden in Fig. 2a. With the rise in the

tunnel overburden from 50 to 500 m, the 95% displacement occurrence range increased by the tunnel diameter. In other words, the 95% displacement occurrence range increased from 1–2 times the tunnel diameter to 2–3 times the tunnel diameter. There was no significant relationship between the occurrence location of 5% displacement and the overburden, and in general, the 5% displacement occurred within the range of 1–2 times the tunnel diameter. It may be caused by the difference in displacement magnitude.

Figure 2b shows the location of 5 and 95% displacement versus cohesion. In order to clarify the diagram and eliminate the impact of the overburden, the overburden was chosen equal to 250 m. The same trend was also considered for the other overburdens. As can be seen, there was no significant relationship between the occurrence location of the 95% displacement and the cohesion, and the range of the mentioned displacement was 1.5–2.5 times the tunnel diameter. With the rise in the cohesion, the change in the location of the 5% displacement increased by the tunnel diameter. In other words, the range of changes altered from 1.2 to 1.4 times the tunnel diameter to 1.6–2.8 times it. The internal friction angle had no effect on the occurrence location of 5 and 95% displacement. It was found that the location of 5 and 95% displacements was affected by the tunnel overburden.

Although the deformation modulus, internal friction and cohesion are the controlling factors of the tunnel displacement magnitude, when the tunnel displacement is normalized based on total displacement to extract tunnel displacement profile, these parameters do not have a significant relation with occurrence location of 5% and 95% displacement. The cohesion just affects the occurrence location of 5% displacement which may be as a result of tunnel face supporting effect.

Table 2 Analysis of variance at 95% of tunnel displacement

Parameter under investigation	DF	SS	MS	F	P
Tunnel diameter	1	4.379	4.3794	82.75	0.000
Overburden	2	75.312	37.656	711.52	0.000
Friction angle	2	8.207	4.1035	77.54	0.000
Young modulus	3	0.211	0.0704	1.33	0.265
Cohesion	3	9.853	3.2843	62.06	0.000

DF degree of freedom, *SS* sum of squares, *MS* mean square, *F* F-fisher, *P* significance level calculated based on F

2.2.2 The Effect of Changes in Geomechanical Parameters, Diameter, and Overburden on the Face Displacement

As mentioned earlier, the amount of displacement in the face is one of the key points of the longitudinal profile of a tunnel, which is reported to be 25–30% of the total displacement of the tunnel. Based on the numerical modeling results, the amount of displacement in the tunnel face changed by changing the geomechanical parameters shown in Table 1. For the overburden of 50–500 m and tunnel diameter of 7 m, the range was 18–32%, with an average of 27%, while for the diameter of 10 m, it changed in the range of 20–28% with an average of 26%. Figure 3 shows the effect of cohesion on the percentage of displacement in the face for diameters of 7 and 10 m. For both diameters, the increase in cohesion led to a limitation of the range of changes in the percentage of displacement in the face and an increase in its average value with an increase in cohesion. The increase in diameter also limited the range of changes in the percentage of displacement in the face by about 5%, but the average percentage of displacement in the face was almost independent of the rise in diameter, experiencing a reduction by only 1%. The upper limit of the percentage of displacement in the face was independent of the increase in cohesion, being about 31 and 28% for the diameters of 7 and 10 m, respectively. However, the lower limit of the change in the percentage of displacement in the face increased with cohesion rise. The lower limit increased from 18 to 25% for the diameter of 7 m, while raising from 20 to 26% for the diameter of 10 m.

Due to the limited range of changes in the percentage of displacement in the face for the diameter of 10 m, especially with the rise in the cohesion, the effect of other parameters, such as internal friction angle, deformation modulus, and overburden was limited and negligible. For more clarification, the percentage of displacement occurred in the face were plotted versus the overburden and cohesion when the tunnel diameter is 10 m (Fig. 4). As it is clear, the average value of displacement in the face is almost the same when the overburden is risen from 50 to 500 m. In addition, the percentage of displacement in the face slightly increased whit increasing the cohesion.

For the diameter of 7 m, the changes in the percentage of displacement in the face are plotted versus overburden and shown in Fig. 4. Unlike cohesion, the rise in overburden resulted in a decreasing trend in the face displacement. For example, at 50 kPa cohesion, the average displacement percentage in the face decreased from 30 to 20% with increasing the overburden. The increasing trend of the percentage of displacement in the face was also evident with the growth of cohesion in this diagram, and this trend was almost the same for the overburdens of 250 and 500 m, while having a slight increasing trend in the overburden of 50 m, at which the upper bound of the change in face displacement was constant, being equal to 31%. In other words, in low overburden, the role of cohesion on the percentage of displacement released at the face was lower. In general, for the diameter of 7 m, the percentage of displacement in the face was a function of cohesion and overburden, being inversely related to overburden and directly related to cohesion, while for the diameter of 10 m, it was only a function of cohesion (Fig. 5).

Fig. 2 Occurrence location
of 5 and 95% of total
displacements which is
normalized using tunnel
diameter; **a** versus tunnel
overburden, **b** versus
cohesion for overburden
250 m
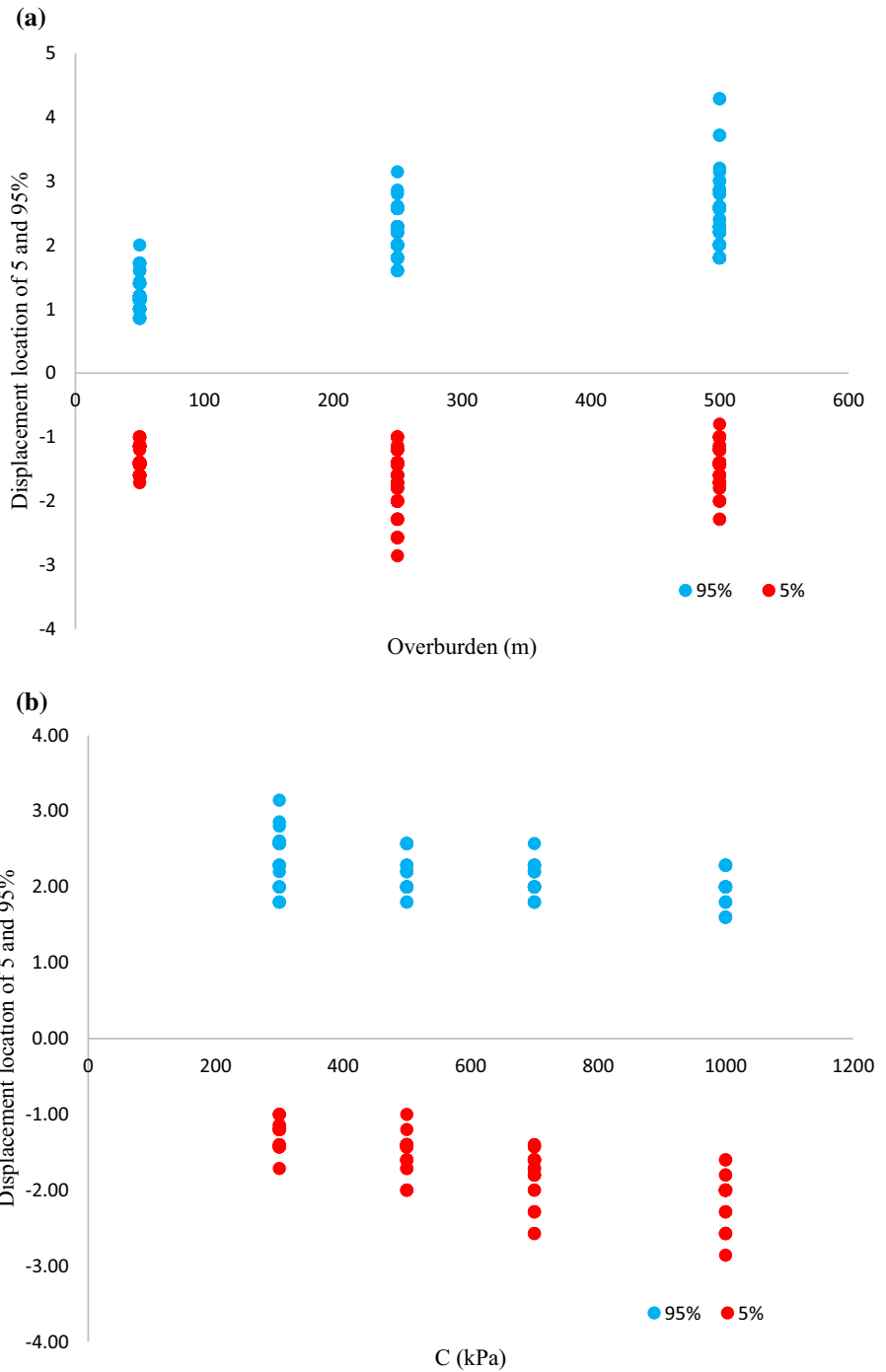
Fig. 3 The effect of increased cohesion on the percentage of displacement in the face for the diameters of 7 and 10 m
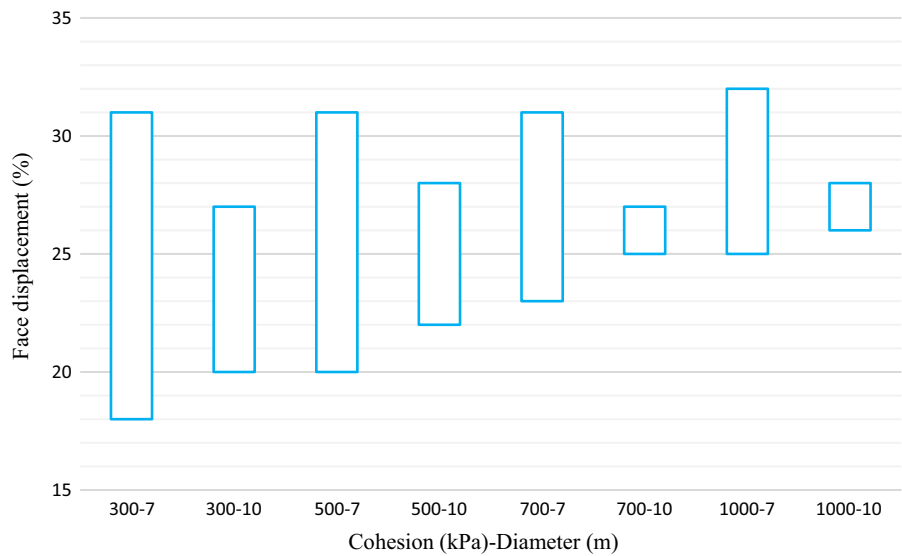
Fig. 4 The effect of cohesion increment on the percentage of displacement in the face for overburdens of 50–500 m and the diameter of 10 m
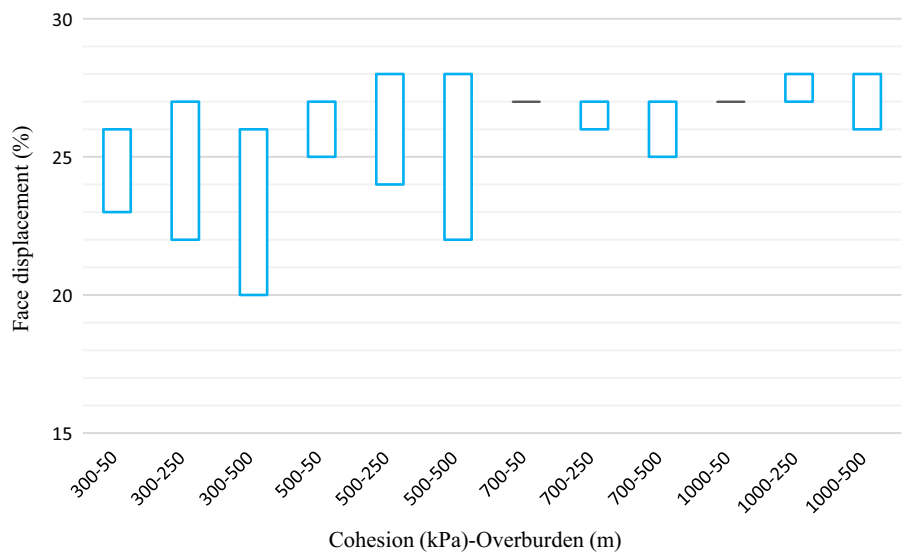

2.2.3 Effect of changes in geomechanical parameters, diameter, and overburden on tunnel displacement profile

To investigate the tunnel displacement profile and the possibility of comparing the obtained displacement profile with the displacement profile provided by Hoek, the amount of tunnel crown displacement was normalized relative to the maximum displacement, the distance from the face was normalized relative to the tunnel diameter, and the displacement (%) against the distance from the normalized face is depicted.

Figure 6 demonstrates the displacement profile obtained from the numerical simulation, along with the displacement profile proposed by Hoek (Rocscience 2000–9).

Changes in geomechanical parameters, overburden, and tunnel diameter led to changes in displacement profile. The function proposed by Hoek [Eq. (1)] was used to investigate the effect of the mentioned parameters on the displacement profile. The constant coefficients of this function, including C_1 to C_4, which are shown in Eq. (2), were evaluated by fitting the function to the displacement profile, using numerical

Fig. 5 The effect of a rise in cohesion on the percentage of displacement in the face for overburdens of 50–500 m and the diameter of 7 m
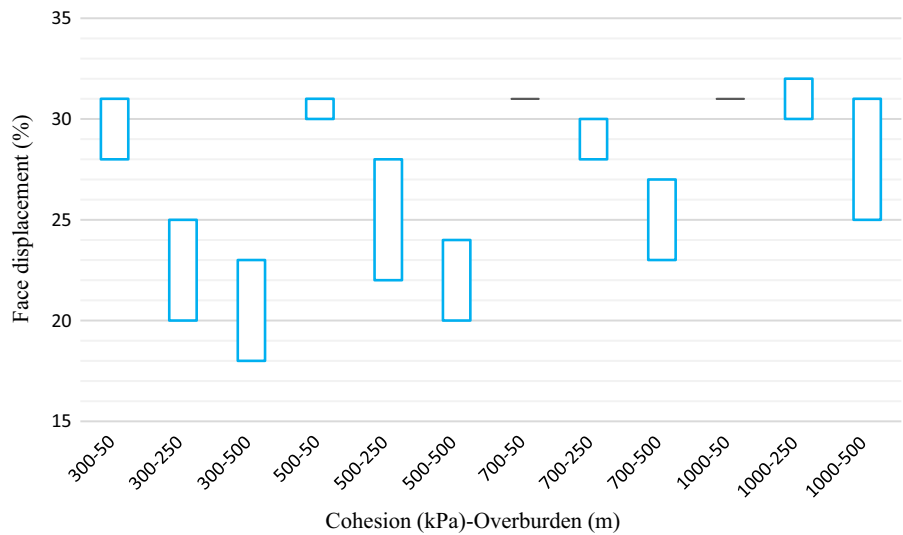
Fig. 6 Tunnel displacement profile against Hoek's proposed displacement profile
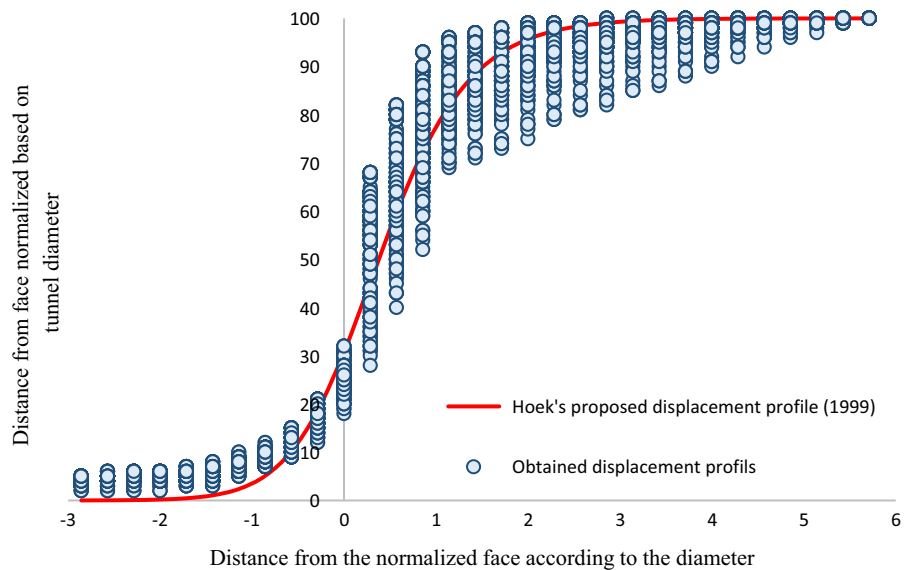
simulation and MATLAB software. By using the analysis of variance, the results of which are shown in Table 3, the relationship between the constant coefficients C_1–C_4 and the variables used in the numerical simulation, including overburden, tunnel diameter, deformation modulus, cohesion, and internal friction angle was evaluated.

$$Y = \frac{100}{[1 + e^{-(X/0.55)}]^{1.7}} \tag{1}$$

$$Y = \frac{C_1}{[C_2 + e^{-(X/C_3)}]^{C_4}} \tag{2}$$

where Y is the tunnel displacement in percentage, which is normalized with respect to the maximum displacement, X is the distance from the face, which is normalized relative to the tunnel diameter, and C_1–C_4 are constant coefficients.

According to the results of the analysis of variance, there was no significant relationship between any of the variables used in numerical simulation and coefficient C_1. The coefficient C_1 was considered equal to 75, while it was 100 in Hoek's proposed profile. The coefficient C_2 was affected by overburden, and other parameters had no significant relationship with

Table 3 Analysis of variance of constant coefficients C_1–C_4

Coefficient	Parameter	DF	SS	MS	F	P
C1	Diameter	1	204.3	204.3	0.55	0.459
	Overburden	2	1076.3	538.1	1.45	0.236
	Cohesion	3	1126.9	375.6	1.01	0.387
	Friction angle	2	639.6	319.8	0.86	0.423
	Young modulus	3	1674.6	558.2	1.51	0.213
C2	Diameter	1	0.00009	0.00009	0.00	0.966
	Overburden	2	0.70745	0.35373	6.85	0.001
	Cohesion	3	0.35073	0.11691	2.27	0.081
	Friction angle	2	0.14945	0.07472	1.45	0.237
	Young modulus	3	0.25598	0.08533	1.65	0.177
C3	Diameter	1	1.08356	1.08356	383.13	0.000
	Overburden	2	3.32619	1.66310	588.04	0.000
	Cohesion	3	0.47771	0.15924	56.30	0.000
	Friction angle	2	0.18976	0.09488	33.55	0.000
	Young modulus	3	0.00427	0.00142	0.50	0.680
C4	Diameter	1	2.0734	2.0734	35.31	0.000
	Overburden	2	8.6499	4.3249	73.65	0.000
	Cohesion	3	3.9620	1.3207	22.49	0.000
	Friction angle	2	0.3217	0.1609	2.74	0.066
	Young modulus	3	0.1484	0.0495	0.84	0.472

coefficient C_2. The coefficient C_3 was affected by the overburden, diameter, cohesion, and internal friction angle, and the only parameter that did not affect it was the deformation modulus. The coefficient C_4 was also affected by overburden, cohesion, and tunnel diameter. The ineffectiveness of the deformation modulus on the displacement profile was also confirmed in the previous subsections, and the internal friction angle had a slight effect on the displacement profile. The nonlinear multivariate regression analysis was performed to investigate the effect of overburden, diameter, cohesion, and angle of internal friction on tunnel displacement profile and extract profiles proportional to the geomechanical parameters, diameter, and overburden. Equations (3)–(5) are the most suitable functions to estimate the coefficients C_2, C_3, and C_4. The criterion for selecting the functions was their simplicity and correlation coefficient. These functions can assist tunnel designers in more accurately assessing the tunnel displacement profile, the internal forces of the installed support, and the surface settlement.

$$C_2 = -7 \times 10^{-6}H^2 + 5 \times 10^{-3}H + 0.151 \quad R^2 = 1 \tag{3}$$

$$C_3 = e^{\left(-9.54 \times 10^{-2}D + 1.2 \times 10^{-3}H - 4.41 \times 10^{-4}C - 0.015\varphi + 0.38\right)} \\ R^2 = 0.83 \tag{4}$$

$$C_4 = e^{\left(-5 \times 10^{-2}D + 6.85 \times 10^{-4}H - 2 \times 10^{-4}C + 0.58\right)} \quad R^2 = 0.63 \tag{5}$$

where H is the overburden (m), D is the tunnel diameter (m), φ is the internal friction angle (°), and C is the cohesion (kPa).

3 Conclusion

Investigations on tunnel displacement profiles obtained from numerical simulations led to the following results:

Although the deformation modulus affected the amount of maximum displacement, it had no effect on the tunnel displacement profile, which was normalized

with respect to the maximum displacement and tunnel diameter.

Overburden and tunnel diameter were the two main parameters affecting the occurrence location of displacement of 5 and 95%. The cohesion also affect'ted the occurrence location of 5% displacement. The location of the 5% displacement was in the range of − 2.86 to − 0.8 times the tunnel diameter, and the location of the 95% displacement was in the range of 0.86–4.29 times of the tunnel diameter.

The percentage of displacement released on the face was 27% on average for the diameter of 7 m and 26% for the diameter of 10 m. Increased cohesion limited the range of changes in the percentage of displacement released in the face and increased its average value.

The percentage of displacement released in the face decreased with increasing the overburden. Parameters influencing the percentage of displacement released in the face included overburden, tunnel diameter, and cohesion. For the diameter of 10 m, the effect of overburden on the displacement released in the face was limited in comparison with the diameter of 7 m.

To compare the results of the present study with previous studies, the displacement profile proposed by Hoek was fit with the displacement profile obtained from numerical simulation, and regression analysis was performed on the fixed coefficients of the fit function. The results showed that the value of coefficient C_1 was independent of the variables used in numerical simulation, and its average value was 75. The coefficient C_2 was a function of overburden; the coefficient C_3 is a function of overburden, cohesion, diameter, and internal friction angle, and the coefficient C_4 was a function of overburden, cohesion, and tunnel diameter. In order to evaluate the mentioned coefficients, functions with acceptable correlation coefficients were presented, which can be helpful in more accurately predicting the tunnel displacement profile.

Declarations

Conflict of interest The authors declare that they have no conflict of interest.

References

Rahim HHA, Enieb M, Abdelmoamen Khalil A, Ahmed ASH (2015) Twin tunnel configuration for Greater Cairo metro line No. 4. Comput Geotech 68:66–77. https://doi.org/10.1016/j.compgeo.2015.03.015

Addenbrooke TI, Potts DM (2001) Twin tunnel interaction: surface and subsurface effects. Int J Geomech 1(2):249–271

Attewell PB, Yeates J, Selby AR (1986) Soil movements induced by tunnelling and their effects on pipelines and structures. Blackie, Glasgow

Carranza-Torres C, Fairhurst C (2000) Application of the convergence-confinement method of tunnel design to rock masses that satisfy the hoek-brown failure criterion. Tunn Undergr Space Technol 15(2): 187–213. https://doi.org/10.1016/S0886-7798(00)00046-8

Carranza-Torres C, Fairhurst C (1999) The elasto-plastic response of underground excavations in rock masses that satisfy the Hoek–Brown failure criterion. Int J Rock Mech Min Sci 36(6):777–809

Chakeri H, Hasanpour R, Hindistan MA, Ünver B (2011) Analysis of interaction between tunnels in soft ground by 3D numerical modeling. Bull Eng Geol Env 70(3):439–448. https://doi.org/10.1007/s10064-010-0333-8

Chen SL, Lee SC, Gui MW (2009) Effects of rock pillar width on the excavation behavior of parallel tunnels. Tunn Undergr Space Technol 24(2):148–154. https://doi.org/10.1016/j.tust.2008.05.006

Do N-A, Dias D, Oreste P, Djeran-Maigre I (2014) Three-dimensional numerical simulation of a mechanized twin tunnels in soft ground. Tunn Undergr Space Technol 42:40–51. https://doi.org/10.1016/j.tust.2014.02.001

Gao X, Wang HN, Jiang MJ (2021) Analytical solutions for the displacement and stress of lined circular tunnel subjected to surcharge loadings in semi-infinite ground. Appl Math Model 89:771–791. https://doi.org/10.1016/j.apm.2020.07.061

Ghaboussi J, Ranken RE (1977) Interaction between two parallel tunnels. Int J Numer Anal Methods Geomech 1(1):75–103. https://doi.org/10.1002/nag.1610010107

Hasanpour R, Chakeri H, Ozcelik Y, Denek H (2012) Evaluation of surface settlements in the Istanbul metro in terms of analytical, numerical and direct measurements. Bull Eng Geol Env 71(3):499–510. https://doi.org/10.1007/s10064-012-0428-5

Hoek E (1999) Support for very weak rock associated with faults and shear zones. In: Rock support and reinforcement practice in mining, pp 19–32

Kong F, Lu D, Du X, Li X, Su C (2021) Analytical solution of stress and displacement for a circular underwater shallow tunnel based on a unified stress function. Ocean Eng 219:108352. https://doi.org/10.1016/j.oceaneng.2020.108352

Lu D, Kong F, Du X, Shen C, Gong Q, Li P (2019) A unified displacement function to analytically predict ground deformation of shallow tunnel. Tunn Undergr Space Technol 88:129–143. https://doi.org/10.1016/j.tust.2019.03.005

Lu D, Kong F, Du X, Shen C, Su C, Wang J (2020) Fractional viscoelastic analytical solution for the ground displacement of a shallow tunnel based on a time-dependent unified displacement function. Comput Geotech 117:103284. https://doi.org/10.1016/j.compgeo.2019.103284

Moussaei N, Khosravi MH, Hossaini MF (2019) Physical modeling of tunnel induced displacement in sandy grounds. Tunn Undergr Space Technol 90:19–27. https://doi.org/10.1016/j.tust.2019.04.022

Ocak I (2008) Control of surface settlements with umbrella arch method in second stage excavations of Istanbul Metro. Tunn Undergr Space Technol 23(6):674–681

RocSupport Tutorial Manual(2009) Rock support interaction and deformation analysis for tunnels in weak rock. Rocscience Inc

Song G, Marshall AM (2020) Centrifuge modelling of tunnelling induced ground displacements: pressure and displacement control tunnels. Tunn Undergr Space Technol 103:103461. https://doi.org/10.1016/j.tust.2020.103461

Unlu T, Gercek H (2003) Effect of Poisson's ratio on the normalized radial displacements occurring around the face of a circular tunnel. Tunn Undergr Space Technol 18(5):547–553

Wang HN, Chen XP, Jiang MJ, Song F, Wu L (2018) The analytical predictions on displacement and stress around shallow tunnels subjected to surcharge loadings. Tunn Undergr Space Technol 71:403–427. https://doi.org/10.1016/j.tust.2017.09.015

Wang HN, Zeng GS, Utili S, Jiang MJ, Wu L (2017) Analytical solutions of stresses and displacements for deeply buried twin tunnels in viscoelastic rock. Int J Rock Mech Min Sci 93:13–29. https://doi.org/10.1016/j.ijrmms.2017.01.002

Wang J, Li E, Chen L, Wang J, Tan Y, Duan J, Pu S, Gao L, Han Y, Wang C (2019) Measurement and analysis of the internal displacement and spatial effect due to tunnel excavation in hard rock. Tunn Undergr Space Technol 84:151–165. https://doi.org/10.1016/j.tust.2018.11.001

Yertutanol K, Akgun H, Sopacı E (2020) Displacement monitoring, displacement verification and stability assessment of the critical sections of the Konak tunnel, İzmir, Turkey. Tunnel Undergr Sp Technol 101:103357. https://doi.org/10.1016/j.tust.2020.103357

Zeng GS, Wang HN, Jiang MJ, Luo LS (2020) Analytical solution of displacement and stress induced by the sequential excavation of noncircular tunnels in viscoelastic rock. Int J Rock Mech Min Sci 134:104429. https://doi.org/10.1016/j.ijrmms.2020.104429

Zhang M, Li S, Li P (2020) Numerical analysis of ground displacement and segmental stress and influence of yaw excavation loadings for a curved shield tunnel. Comput Geotech 118:103325. https://doi.org/10.1016/j.compgeo.2019.103325

Zheng G, Yang P, Zhou H, Zeng C, Yang X, He X, Yu X (2019) Evaluation of the earthquake induced uplift displacement of tunnels using multivariate adaptive regression splines. Comput Geotech 113:103099. https://doi.org/10.1016/j.compgeo.2019.103099

Zheng M, Li S, Zhao H, Huang X, Qiu S (2021) Probabilistic analysis of tunnel displacements based on correlative recognition of rock mass parameters. Geosci Front 12(4):101136. https://doi.org/10.1016/j.gsf.2020.12.015